Application of a Simple Image Velocimetry Algorithm in hydrometry

Preprint · July 2020

DOI: 10.13140/RG.2.2.20897.43364

5 authors, including:

Evangelos Rozos
National Observatory of Athens
61 PUBLICATIONS **677** CITATIONS
SEE PROFILE

Panayiotis Dimitriadis
National Technical University of Athens
129 PUBLICATIONS **598** CITATIONS
SEE PROFILE

Katerina Mazi
National Observatory of Athens
33 PUBLICATIONS **448** CITATIONS
SEE PROFILE

Antonis D. Koussis
National Observatory of Athens
149 PUBLICATIONS **1,734** CITATIONS
SEE PROFILE

Application of a Simple Image Velocimetry Algorithm in hydrometry

Evangelos Rozos[1,*], Panayiotis Dimitriadis[1], Katerina Mazi[1], Spyridon Lykoudis[1], Antonis Koussis[1]

[1] Institute for Environmental Research & Sustainable Development, National Observatory of Athens, Greece
* Correspondence: erozos@noa.gr; Tel.: +30-2108-09125 (GR)

Abstract: The measurement of river discharge under various conditions is of paramount importance in hydrology. The traditional method to make a discharge measurement, and the only option until recently, is very tedious and sometimes even dangerous. For this reason, nowadays, remote sensing techniques are employed to reduce the need for traditional discharge measurements. Image velocimetry is a low-cost remote sensing technique that is capable of providing the spatial distribution and temporal variation of the surface flow velocities. In this manuscript, a simple, fast, and open-source method is presented that employs the LSPIV method to estimate the flow velocities along a cross-section from a video. This method is applied to four case studies. The results of these applications are analyzed statistically to examine whether the identification of the statistical structure of the surface velocities can help to estimate the average flow velocity of the cross-section.

Keywords: stream discharge, remote sensing, image velocimetry, LSPIV, statistical analysis

---

1. Introduction

The measurement of river discharge under various conditions is of paramount importance in hydrological applications [1, 2, 3]. The standard method to make a discharge measurement involves a series of water depth and velocity measurements in various segments of a cross-section in order to apply the following equation (see Eq. 5.1 in [4]):

$$Q = \sum a_i v_i, \text{ with } i = 1 \dots n \quad (1)$$

where Q is the total discharge, a_i is the area of the i^{th} segment of the measured cross-section, v_i is the average velocity of the i^{th} segment of the measured cross-section, and n is the number of segments in which the cross-section is divided (no fewer than 10 in most rivers, and at least 25 for wide rivers [4]). It becomes evident that the traditional method, where measurements are taken manually with a current meter, is tedious and, when the flow velocity is high, as in flooding conditions, prohibitively dangerous.

A modern technique that is based on the Doppler effect is the acoustic Doppler current profiler (ADCP). This technique employs a float on which acoustic transducers, GPS, and other equipment are mounted. The float is dragged along a cross-section to simultaneously perform bathymetry and velocity measurements. The result is the velocity field over the depth and along the cross-section [5, 6]. The integration of this field gives the total discharge. This equipment is currently very expensive (tens of thousands of Euros).

Two other popular, and less expensive, remote sensing techniques are the surface flow velocity radar (SVR) and the image-based method. Both methods provide only surface velocities. For this reason, some statistical analysis should be employed to obtain the probability distribution of the velocity, from which the velocity profile (over the depth) can be obtained [7, 8, 9]. SVR requires specialized equipment and provides measurements only at specific predefined locations. On the other hand, the image-based method does not require any specialized equipment, other than the ubiquitous smartphone camera, and can estimate the distribution of the flow velocities over a selected region of interest. For this reason, the image-based method, known also as image

velocimetry, is becoming increasingly popular mainly both because of its low cost and of the sensor simplicity (a simple camera). The latter translates into low weight equipment, which allows the application of this method even from light unmanned aerial vehicles (UAV) [10].

As mentioned above, the core procedure of the image velocimetry is the processing of the obtained images (usually the frames of a video). The processing algorithms are classified into two main categories: those based on particle tracking (e.g., Large-Scale Particle Tracking Velocimetry, Kanade–Lucas Tomasi, Optical Tracking Velocimetry, etc.), and those based on cross-correlation maximization (e.g., Large-Scale Particle Image Velocimetry, Surface Structure Image Velocimetry, etc.). An extensive review of these methods, and the corresponding tools, can be found in [11, 12, 13].

The software required for the image velocimetry is highly specialized. For example, PIVlab is freely available [14], but requires commercial software (MATLAB). OpenPTV is available on many development platforms (Python, MATLAB, C++), but has not been implemented in MS Windows. DischargeProcessing of Photrack AG is a commercial product. Additionally, some of these tools require a considerable amount of time to complete the image processing. An interesting option is Fudaa-LSPIV [15]. Fudaa-LSPIV employs Java for providing a user-friendly interface, but the processing algorithms are written in FORTRAN in order to achieve maximum performance. It is available in both Windows and Linux operating systems.

LSPIV has been applied in engineering applications since 1998 [16], and is the most widely used and documented methodology [11, 17]. According to Le Boursicaud et al. [18] LSPIV provides reliable longitudinal flow velocity estimations even with home movies that can be found in social media. Dramais et al. [19] embraced the idea of using LSPIV to improve the accuracy of rating curves in high discharges. Le Coz et al. [20] applied LSPIV in a Mediterranean river for a wide range of discharges and found good agreement with the velocities obtained by ADCP (±10%). Kantoush et al. [21] have demonstrated the efficiency of LSPIV in a variety of engineering applications.

In this study, we suggest a simple image velocimetry tool based on the LSPIV method. This tool is developed in MATLAB and is freely available [22]. We find advantageous the development of such a tool inside a numerical computing environment because it facilitates greatly a statistical analysis of the results. Our tool is compatible with MATLAB, but also with the open-source Octave, which means that it can be applied without requiring installation of any commercial software. Furthermore, the code of our tool is only 20 kB (the PIVlab code is 500 kB, most of it dedicated to the user interface). This allows other researchers to easily understand our code and modify it according to their requirements. Though we have not performed extensive benchmarking, our algorithm appears to be quite fast. PIVlab required 15 min to perform image analysis on 200 frames [13] to derive the velocity field over an area of 150 m^2. Our algorithm required 75 seconds (using MATLAB) for analyzing 500 HD frames to derive the velocity profile along the line of the cross-section (analysis run on a 3.5 GHz dual-core CPU laptop). It should be noted that if the processing speed is of high importance, then an approach that employs native code for the CPU-intensive algorithms (e.g., Fudaa-LSPIV) could be a better choice. Therefore, studies that involve non-time-critical image velocimetry could benefit from our algorithm, especially if there are no resources for commercial software or if new ideas on image velocimetry are to be tested.

The suggested tool is applied in four case studies. The results of these applications are analyzed statistically to examine if it is possible to derive a characteristic hydraulic property of a cross-section that can be related to the average velocity. The most common approach is to link the average to the maximum velocity of a cross-section [7], which in most natural rivers occurs at or near the water surface (for a review see [8, 9]). However, these methods require the determination of an additional parameter (often symbolized as M) for the characterization of the streamflow. It has been observed that the average velocity of the cross-section may be obtained from the average surface velocity with a standardized error of around 10% [9, 23, 24]. Thus, here, we investigate the efficiency of two estimators: a) a fraction of the average surface velocity and b) the quantile of the probability distribution of the surface velocity that is close to the average velocity of the cross-section.

2. Methods

2.1. Measure flow velocity from video

In general, image velocimetry includes three steps, image pre-processing, evaluation, and post-processing [25]. Image pre-processing includes applying various filters and operations to the video frames to facilitate motion detection. Image evaluation is applied between successive frames to obtain particle displacements. Finally, in the image post-processing, the velocity vector coordinates are translated from the image coordinate system (rows and columns of pixels) to real-world coordinates. Furthermore, any estimated velocity that significantly exceeds expected values is discarded.

In our study, the image pre-processing includes application of the Gaussian blur filter, image subtraction, conversion to greyscale, and contrast adjustment. More specifically, to remove the noise from the frames (mainly introduced by video compression algorithms), a Gaussian filter is applied. An 11×11 mask is employed with a standard deviation of 1 [26]. Then, the video frame i is subtracted from the frame i+1. This removes the time-invariant information and leaves only the temporal changes in order to facilitate motion detection. The resulting images from this subtraction are converted to greyscale. Finally, a contrast adjustment is applied to the contents of the interrogation and search areas according to a parameter that ranges from 0 to 1. All pixels in the processed area with a value lower than that of the area's maximum multiplied by the contrast adjustment parameter are turned off.

In the image evaluation, motion detection is applied between successive frames to obtain particle displacements (debris, boils, ripples, etc.). The search area and the interrogation area are concentric rectangles, the centres of which lie on the line of the cross-section, where the discharge is to be measured. The orientation of these rectangles is selected to have the long edge parallel to the flow. The higher the flow, the higher should be the ratio of the long to the short edges. To estimate the average particle displacement, the algorithm employs the fast normalized cross-correlation [27] between the contents of the interrogation area in the frame i and the search area in frame i+1. The shift of the interrogation area j contents of the frame i that results in the highest cross-correlation value with the search area j contents of the frame i+1 is assumed to be the average particle displacement in the area j between i and i+1 frames. This highest cross-correlation value should exceed a minimum threshold for the displacement to be considered valid.

Image post-processing derives the flow velocity. The vectors of the previously obtained displacements (vectors in the image coordinate system) are transformed into the real-world coordinate system. For this reason, a mapping from the position of the pixels of the image to real-world coordinates is required. This is called image registration (image registration is a more generic term that refers to transforming sets of data to a specific coordinate system) or orthorectification. This mapping is accomplished with a transformation function. A generic method to build transformation functions has been suggested by Goshtasby [28] that employs a linear combination of orthogonal polynomials. A much simpler approach, when the plane of the camera film is far from and parallel to the scene, is the 'non-reflective similarity' transformation (see Eq. 1 in [29]). To determine the parameters of this transformation, the real-world coordinates of only two control points of the image are required. If the position of the camera does not satisfy the previous conditions, then the 'projective' transformation should be used instead (see Eq. 3 in [30]). This transformation requires the real-world coordinates of four control points.

In image post-processing, the cases where the maximum cross-correlation is obtained from irrelevant particles are filtered out. For example, suppose that in the frame i the area j contains only one particle just about to exit the area with the flow, and in the frame i+1, the area j contains only one particle just entering the area. This may result in a misleadingly high correlation between these two irrelevant particles. To avoid this, an upper and a lower (can be negative) threshold of acceptable velocity is employed, above which any estimated value is considered unrealistic.

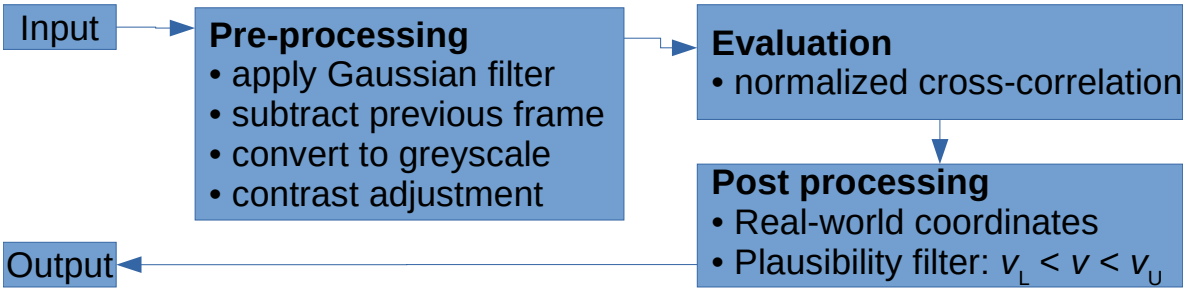

Figure 1: Schematic representation of image velocimetry algorithm

This algorithm (see Figure 1) has been implemented in MATLAB code (also compatible with the open-source platform Octave version 5.1 and later). The algorithm parameters that need to be defined in each application are the video filename, the minimum acceptable correlation, the maximum acceptable displacement, the contrast adjustment parameter, the coordinates of the control points and the corresponding image coordinates, the type of projection, and the dimensions and the location of the interrogation and search areas.

2.2. Conventional measurement of flow

The conventional flow measurements in the case studies were performed with the current meter RedBack. The distance between the verticals of the measurements was 1 m. At each vertical, measurements were taken at 20, 40, 60, and 80% of the depth. Furthermore, the surface velocity was measured employing a hand-held microwave Doppler radar. Flow velocity measurements with the radar were conducted at 3 or 4 locations with equal spans between them.

2.3. Statistical analysis

The statistical analysis of the velocities obtained by the image velocimetry method includes graphical assessment with histogram plots and selection and fitting of the theoretical distribution function.

The histogram is an empirical method to represent approximately the probability density function of the random variable that corresponds to the data. The histograms were plotted following the methodology described in section 5.2 of [31].

The selection and fitting of the theoretical distribution function was performed with the specialized tool EasyFit of MathWave. For each data set, over 55 probability density functions were assessed employing the Anderson-Darling statistic [32], which gives more weight to the tails than the Kolmogorov-Smirnov test. According to this approach, the following metric is used to assess the fitting:

$$A^2 = -n - \tfrac{1}{n} \sum (2i - 1) \left(\ln F(x_i) + \ln(1 - F(x_{n-i+1}) \right), \text{ with } i = 1 \ldots n \quad (2)$$

where F is the hypothesized distribution function, n is the number of data points, and x_i is the value of the i^{th} data point with $x_i \leq x_{i+1}$. For each assessed F, the A^2 metric is used for estimating the parameters of the distribution F according to the minimum-distance estimation procedure [33].

3. Case studies

3.1. Kolubara River

The first case study is from the publication of Pearce et al. [11], who tested 5 image velocimetry methods on two neighbouring cross-sections of the Kolubara River, Serbia. The video was recorded from a UAV with a very high resolution (4k, 239 Mbps). We obtained the reference points graphically from Figure 2 of [11]. The 'similarity' transformation was used (same as 'nonreflective similarity' with the addition of optional reflection). The required three reference points were the two crosses at the locations (coordinates from Figure 2 of [11]) (8.77, 3.57) and (15.96, 3.6), and the ground control point (GCP) at location (26.00, 30.19). The original video included 600 frames at 24

fps, but because of the low flow velocities the video was sub-sampled to produce a video of 4 fps, which according to Pearce et al. [11] achieves the lowest sensitivity to the LSPIV parameters.

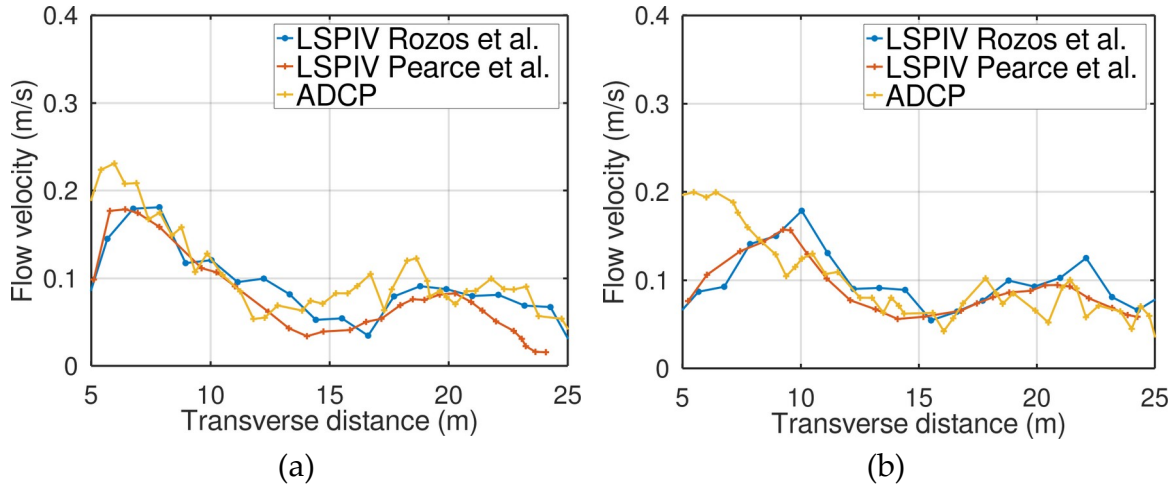

Figure 2: Comparison of LSPIV results obtained by Pearce et al. [11] and by our algorithm at cross-sections S1 (**a**) and S2 (**b**).

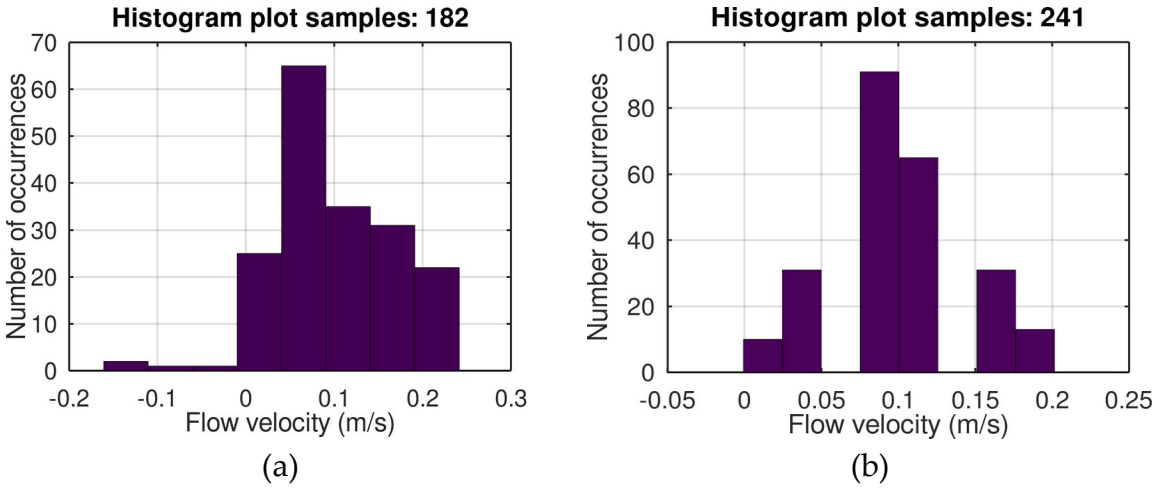

Figure 3: Histograms of the surface velocities at cross-sections S1 (**a**) and S2 (**b**).

The image velocimetry results obtained with our algorithm are compared against those provided in Figure 8 of Pearce et al. [11] for the cross-sections S1 and S2. The profiles of the velocities obtained by our algorithm and by Pearce et al. are displayed in Figure 2. The profiles obtained by the ADCP technique are also provided in Figure 2. The average surface velocity of S1 estimated by our algorithm, Pearce's algorithm, and the ADCP are 0.102, 0.076, and 0.108 m/s respectively. The average surface velocity of S2 estimated by our algorithm, Pearce's, and the ADCP are 0.100, 0.092, and 0.098 m/s respectively. The magnitude of the difference between the two LSPIV algorithms is not greater than the magnitude of the differences between the 5 methods tested by Pearce et al. (see Figure 8 of [11]).

3.2. Loussios river

The second case study is from a cross-section in the Loussios river, Greece (the geographic and hydrological information of this location can be found at https://openmeteo.org/stations/2039/). The shape of the studied cross-section is displayed in Figure 4. Figure 4 also gives the flow measurements obtained with the conventional current meter. Using these measurements in equation (1), the discharge is estimated at 4.77 m^3/s in the cross-section of area 5.34 m^2, and the average velocity is V_{av} = 4.77/5.34 m/s = 0.89 m/s (the arithmetic average is 0.86 m/s).

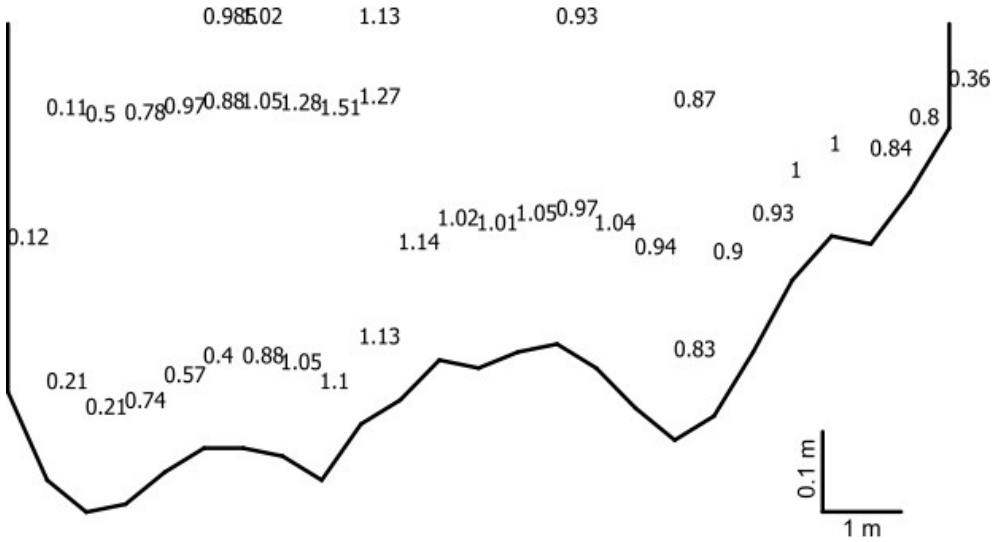

Figure 4: Loussios river cross-section looking downstream. The numbers give the flow velocity (m/s) in the corresponding measurement locations of the cross-section.

The video of the Loussios river was recorded from a bridge over the river with the camera directed vertically downwards. The video quality was HD (17.6 Mbps), it included 500 frames, the frame rate was 30 fps, and the long side of the video was normal to the flow. The minimum acceptable correlation was set equal to 0.85, the contrast adjustment parameter 0.9, the maximum acceptable particle displacement was set equal to 2.0 m/s, the interrogation area size was 70×50 pixels, the search area was 90×60, and 14 areas were used along the cross-section to track the flow.

The 'non-reflective similarity' transformation was employed in the image registration. The required two control points are shown in Figure 5. The first point, A, is set (arbitrarily) to the middle of the lower edge of the frame. This is assumed to be the real-world origin. The x-axis is assumed parallel to the long edge of the frames. This will be the standard practice in all case studies presented here. The next point, B, is set on the y-axis at a distance of 30 cm from A. This distance on the image is estimated from the length of a reference object (the forearm of a human, see the lower right corner in Figure 5).

Figure 5: Loussios river case study. Flow velocity vectors (arbitrary scale) obtained by video processing, and control points (A and B) employed in the 'non-reflective similarity' transformation.

The results of the video processing are shown in Figure 5. Assuming positive y-axis upwards and positive x-axis pointing to the right (along the cross-section in this case study), the average surface flow velocity vector is $(v_x, v_y) = (0.05$ m/s, 1.04 m/s). For comparison, the average flow velocity normal to the cross-section, taking into account the current meter measurements at 0 and 20% of the water depth (from the water surface), was found to be 0.95 m/s (no radar measurements were available for this case study).

Figure 6 displays the histogram of the results of the image velocimetry algorithm (the component v_y). The number of the surface flow velocity vectors obtained by the algorithm was 34.

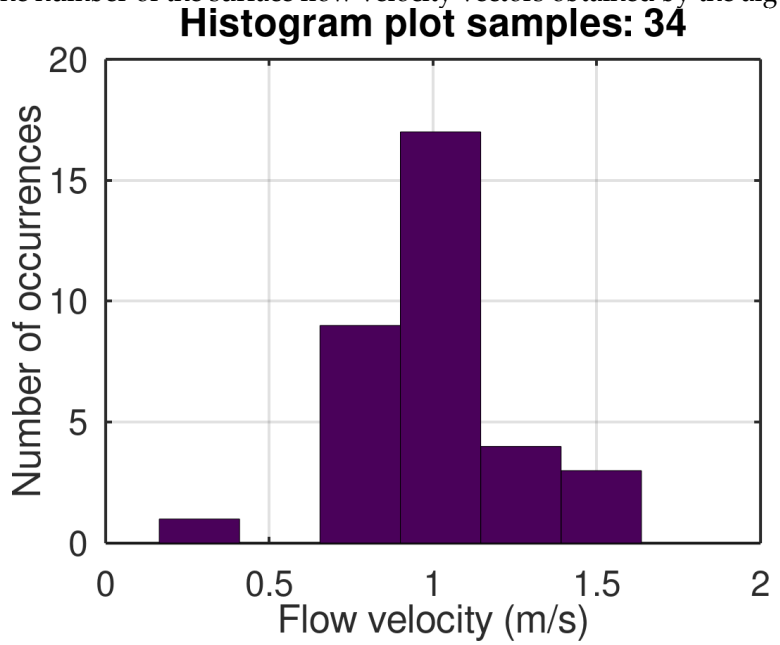

Figure 6: Histogram of the surface velocities obtained by the image velocimetry algorithm at Loussios.

3.3. Nedousa, upper reaches of Nedontas river

The third case study is from a cross-section in the upper reaches of the Nedontas river, from its tributary Nedousa, Greece (see https://openmeteo.org/stations/1487/). The shape of the studied cross-section is displayed in Figure 7. Figure 7 also gives the flow measurements obtained with the conventional current meter. Using these measurements in equation (1) the discharge is estimated at 3.00 m^3/s in the cross-section of area 3.23 m^2, and the average velocity is V_{av}= 3.00/3.23 m/s= 0.93 m/s (the arithmetic average is 0.91 m/s).

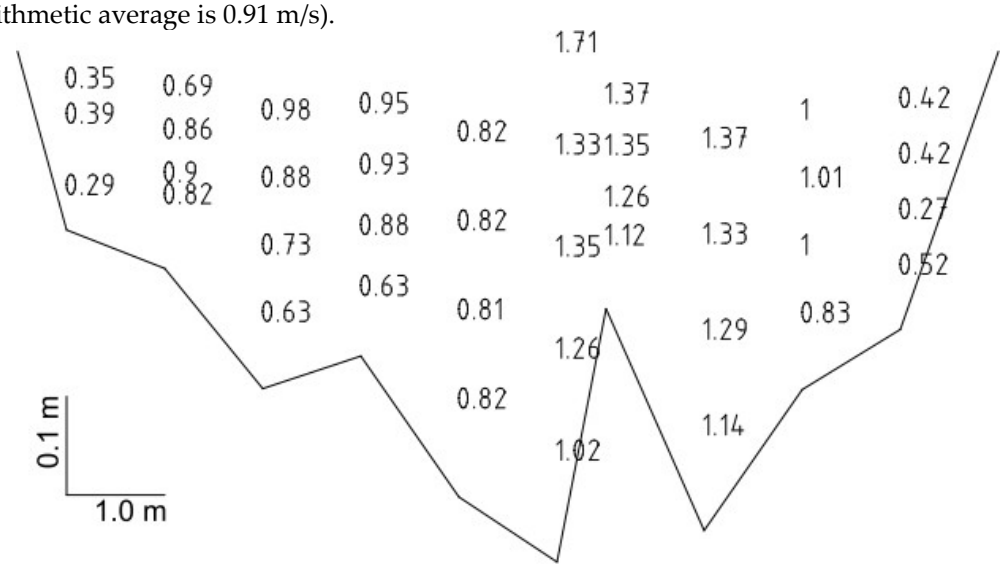

Figure 7: Nedousa cross-section looking downstream. The numbers give the flow velocity (m/s) in corresponding locations of the cross-section.

The video of Nedousa was recorded under a bridge, standing on the right side (looking upstream). The video was recorded in HD (17.3 Mbps), it included 300 frames, the frame rate was 30 fps, and the long side of the video was parallel to the flow. For the video processing, the minimum acceptable correlation was set equal to 0.8, the contrast adjustment parameter 0.8, the maximum acceptable particle displacement was set equal to 3.0 m/s, the interrogation area size was 30×100 pixels, the search area was 80×160, and 20 areas were used along the cross-section to track the flow.

The 'projective' transformation was employed in the image registration. This transformation requires referencing four points. Figure 8 displays the technique employed to obtain the real-world coordinates of the control points. Points B and C are the locations where the hydrologist's right foot meets the water surface when standing a fully-extended arm length away from the cable. Therefore, the x-coordinates of these points equal the arm's length, whereas the y-coordinates are the distances of the hydrologist from the right side of the bridge (looking upstream). Points A and D lie on the water surface at distances from the right bridge side equal to those of B and C respectively, but with x=0 (e.g., in Figure 8, D is the projection of the hydrologist's hand (fist) on the water surface). Having the hydrologist standing this way at two locations across the river flow, the coordinates of four control points can be obtained. It is noted that the image velocimetry does not include the frames with the hydrologist standing to obtain the control points.

The results of the video processing are shown in Figure 8. Assuming that the origin is at the right cable mount (at the bottom of Figure 8, not visible), the y-axis is along the cable (the cross-section) and positive upwards, the positive x-axis points to the right, then the average surface flow velocity vector is $(v_x, v_y) = (-1.32$ m/s, -0.26 m/s). The significant flow along the assessed cross-section ($v_y = -0.26$ m/s) is attributed mainly to the channel expansion at this location. For comparison, the average surface flow velocity normal to the cross-section, taking into account the current meter measurements at 20% of the water depth (from the water surface), was 1.07 m/s. The average surface flow velocity obtained by the hand-held radar was 1.33 m/s (the three measurements were 1.6, 1.5, and 0.9 m/s).

Figure 9 displays the histogram of the results of the image velocimetry algorithm (the component $-v_x$). The number of surface flow velocity vectors obtained by the algorithm was 45.

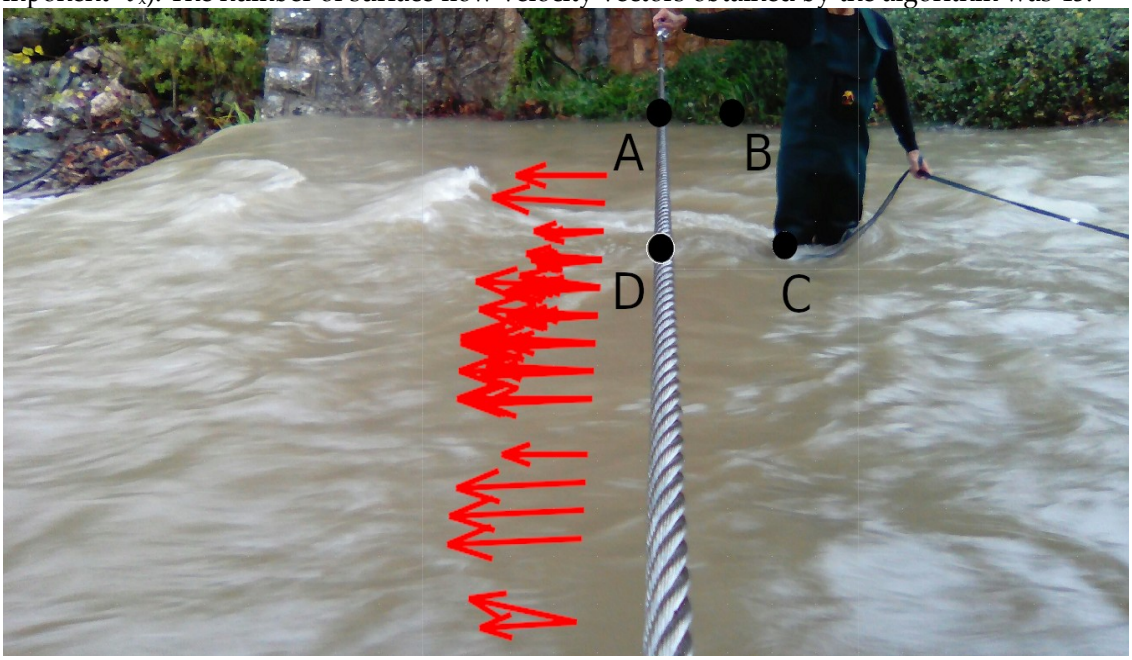

Figure 8: Nedousa case study. Flow velocity vectors (arbitrary scale) obtained by video processing, and control points (A, B, C, and D) employed in the 'projective' transformation.

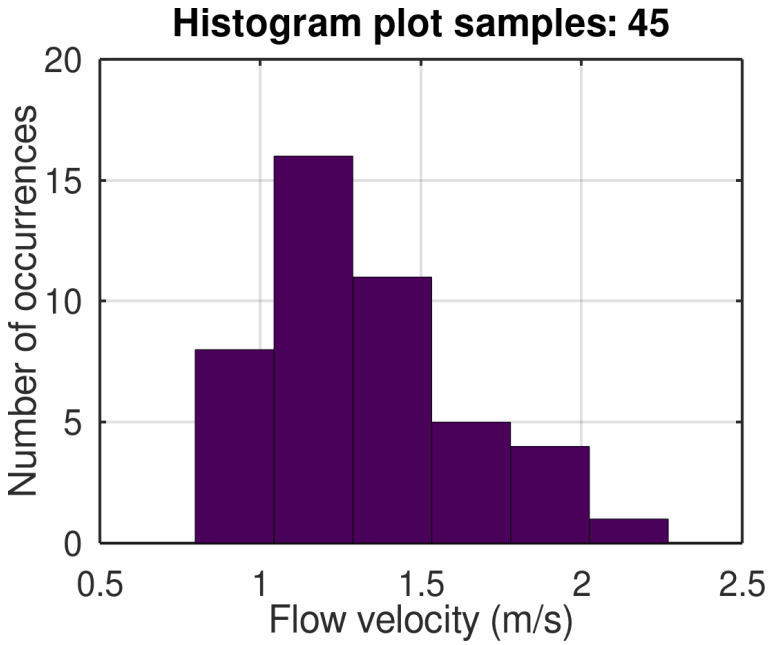

Figure 9: Histogram of the surface velocities obtained by the image velocimetry algorithm at Nedousa.

3.4. Nedontas river, Kalamata city

The fourth case study is from a cross-section close to the Nedontas river mouth, in the city of Kalamata, Greece (the geographic and hydrological information of this location can be found at https://openmeteo.org/stations/1482/). The shape of the studied cross-section is displayed in Figure 10. Figure 10 also gives the flow measurements obtained with the conventional current meter.Using these measurements in equation (1) the discharge is estimated at 4.60 m^3/s in the cross-section of area 1.67 m^2, and the average velocity is V_{av}= 4.60/1.67 m/s= 2.75 m/s (the arithmetic average is 2.52 m/s).

The video of the Nedontas river was recorded under a bridge standing on the left side (looking upstream). The video was recorded in HD (16.2 Mbps), it included 500 frames, the frame rate was 30 fps, and the long side of the video was parallel to the flow. For the video processing, the minimum acceptable correlation was set equal to 0.81, the contrast adjustment parameter 0.9, the maximum acceptable particle displacement was set equal to 7 m/s, the interrogation area size was 50×150 pixels, the search area was 70×250, and 14 areas were used along the cross-section to track the flow.

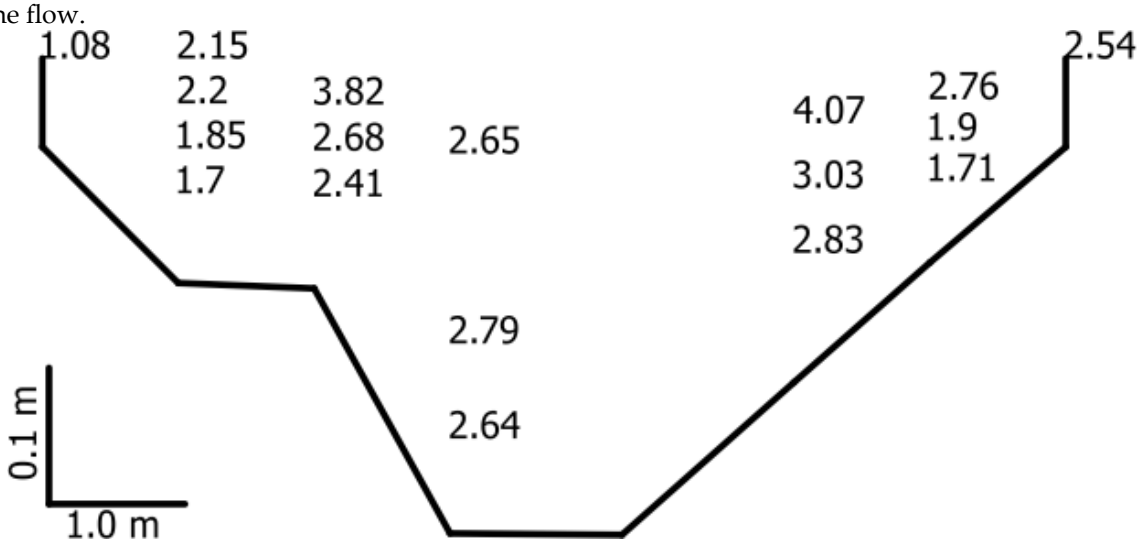

Figure 10: Nedontas river cross-section looking upstream. The numbers give the flow velocity (m/s) in corresponding locations of the cross-section.

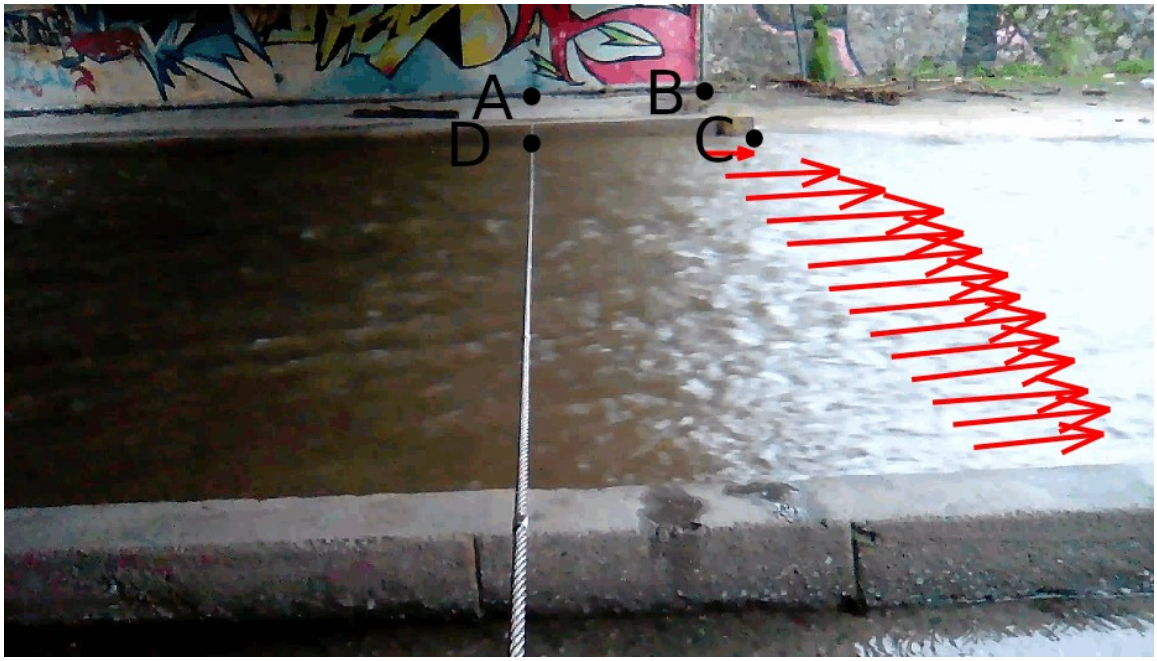

Figure 11: Nedontas river case study. Flow velocity vectors (arbitrary scale) obtained by video processing, and control points (A, B, C, and D) employed in the 'projective' transformation.

The 'projective' transformation was employed in the image registration. This transformation requires referencing four points. Figure 11 displays the technique employed to obtain the real-world coordinates of the control points. In this case, the control points were selected on concrete constructions, so the real-world coordinates of these points were easily measured. It should be noted that, even though there is no water at points A and B, their elevation is only slightly higher than the water surface (formally, all control points should lie on the same plane, the water surface).

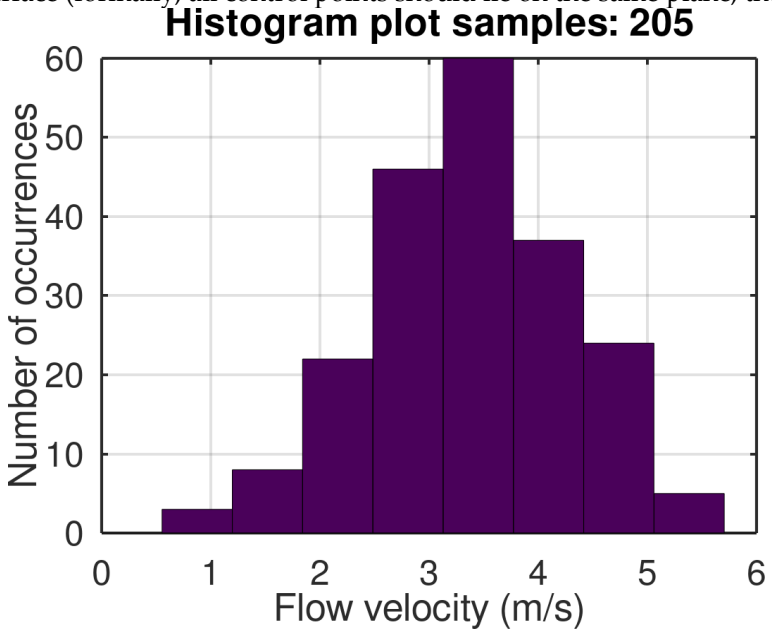

Figure 12: Histogram of the surface velocities obtained by the image velocimetry algorithm at Nedontas.

The results of the video processing are shown in Figure 11. Assuming the origin to be at the left cable mount (at the bottom of Figure 11, not visible), the y-axis along the cable (the cross-section) positive upwards and the positive x-axis pointing to the right, then the average surface flow vector is $(v_x, v_y) = (3.35 \text{ m/s}, -0.10 \text{ m/s})$. The y-component of the flow along the assessed cross-section ($v_y = -0.10$ m/s) is attributed to the transformation errors and to the poorly positioned cable (i.e., the cable, which is assumed as the real-world y-axis, was not positioned normal to the flow). For

comparison, the average surface flow velocity normal to the cross-section, taking into account the current meter measurements at 0 and 20% of the water depth, was 2.66 m/s. However, it is noted that in this case the average surface flow velocity is underestimated because no measurements were taken in the middle part of the cross-section due to the very high flow velocity. The average surface flow velocity obtained by the hand-held radar was 3.83 m/s (four measurements equal to 3.4, 3.8, 4.3, and 3.8 m/s). It is worth noting that the obtained velocity profile from the algorithm suggests, similar to the measurements from the hand-held radar, higher velocities near the centre of the cross-section (Figure 11).

Figure 12 displays the histogram of the results of the image velocimetry algorithm (the component v_x). The number of flow vector velocities obtained by the algorithm was 205.

4. Discussion

Pearce et al. [11] have provided a sensitivity analysis of the LSPIV method on the search and interrogation areas, which they consider to have the greatest impact on the LSPIV method accuracy. The LSPIV method performance remained acceptable for every tested set of parameters. Pearce et al. have studied also the accuracy of five image velocimetry methods. Using the measurements obtained from the ADCP technique as reference values, they found that the LSPIV method offered the best accuracy in most applications with an average Nash-Sutcliffe coefficient of 0.5 (compared to ADCP). It should be noted that according to WMO [4] the ADCP measurements tend to be within 5% of the conventional measurements, whereas the error of the conventional measurements (if well-performed) is 3%.

The case studies highlighted the following difficulties regarding the image velocimetry methodology:

1. If it is not possible to select control points on solid unmistakable locations, their definition may be a challenging procedure requiring improvisation.
2. The 'projective' transformation is prone to errors in the definition of the control points. Inaccurate identification of the real-world coordinates of the control points may result in errors in the estimation of both the magnitude and the direction of the flow vectors.
3. When the camera is not far from and parallel to the scene, i.e., when the 'projective' transformation (see Figures 8 and 11) should be used, areas closer to the camera are recorded with a higher pixel density. Therefore, less reliable information can be derived from the video for the more distant areas.
4. The motion detection of the video processing algorithm is feasible only if the video has recorded a flow with easily detectable moving features (requirement of sufficient seeding density, see [11]). As a rule of thumb, an expert should be able to estimate the flow velocity by watching the video. If this is not so, the image processing algorithm most probably will fail to obtain meaningful results from this video.
5. Despite the previously mentioned disadvantages, the videos requiring 'projective' transformation tend to present a higher effective seeding density, which is essential for the motion detection.
6. The average flow vector, like every 2D vector, has two scalar components, one parallel and one normal to the flow. Occasionally, the video processing algorithm may estimate a non-zero component normal to the flow. If the flow is uniform, this is usually because of errors introduced by the transformation, especially in the 'projective' transformation. This error is acceptable if the erroneously estimated component normal to the flow has only a minor impact on the direction and magnitude of the flow velocity vector.
7. The maximum acceptable displacement, the minimum acceptable correlation, the contrast adjustment parameter, and the interrogation and search area sizes are hyper-parameters that require expertise to select optimal values.

The data of all 5 cross-sections were analyzed statistically employing equation (2). The results of this analysis are displayed in Figure 13 and Table 1.

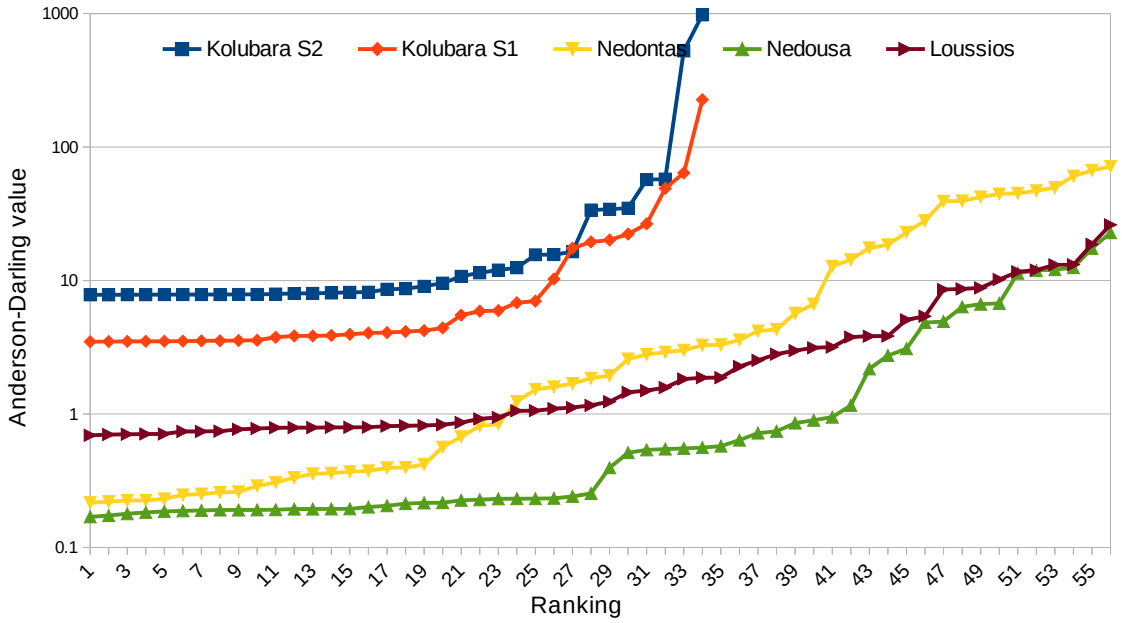

Figure 13: Ranking of 60 distribution functions according to the corresponding value of the Anderson-Darling test.

The lines in Figure 13 appear to be horizontal for a considerable number of distributions. This suggests that a wide variety of distributions fit well to the surface velocities (the scalar component parallel with the flow). During the statistical analysis it was found out that an early jump in these lines (very few distributions fit well to the data) was an indication of an inappropriate upper or lower velocity threshold (see plausibility filter in Figure 1).

It should be noted that the minimum length that can be measured in an image is that corresponding to one pixel. As a result, the displacements obtained from two successive images are discretized. In the case of the 'non-reflective similarity' transformation, the relation of a pixel to the real-world length is constant. Then, and because of the discretization, the obtained velocities (the scalar components of the vector) take values from a limited set, which explains the two gaps in Figure 3b. However, in the 'projective' transformation, the relation of a pixel to the real-world length is defined by a scaling factor that depends on the location in the image. As a result, the obtained velocities take values from a continuous space.

Table 1: Ranking of the best 10 distribution functions according to the Anderson-Darling test.

	Loussios	**Nedontas**	**Nedousa**	**S1**	**S2**
1	Burr (4P)	Error	Gen. Extreme Value	Lognormal (3P)	Johnson SB
2	Dagum (4P)	Fatigue Life (3P)	Log-Pearson 3	Fatigue Life (3P)	Erlang (3P)
3	Log-Logistic (3P)	Beta	Johnson SB	Inv. Gaussian (3P)	Pearson 6 (4P)
4	Logistic	Normal	Pearson 6	Normal	Gamma (3P)
5	Johnson SU	Inv. Gaussian (3P)	Pearson 5	Gen. Gamma (4P)	Beta
6	Gen. Gamma (4P)	Johnson SB	Pearson 5 (3P)	Pearson 6 (4P)	Gen. Gamma (4P)
7	Hypersecant	Gen. Gamma (4P)	Lognormal (3P)	Erlang (3P)	Fatigue Life (3P)
8	Beta	Gen. Extreme Value	Fatigue Life	Pearson 5 (3P)	Lognormal (3P)
9	Fatigue Life (3P)	Lognormal (3P)	Inv. Gaussian (3P)	Gamma (3P)	Burr (4P)
10	Normal	Log-Logistic (3P)	Lognormal	Gen. Extreme Value	Weibull (3P)

The non-exceedance probabilities of the surface velocities of the Loussios, Nedousa, and Nedontas for the corresponding value of V_{av} are 25, 18, and 16% respectively. The average is 20%. It was examined whether the 20th percentile of the surface velocity obtained from the empirical distribution, V_{EMP}, and the best distribution of Table 1, V_{DIS}, can serve as an estimator of V_{av}. The accuracy of this method was tested against the classical method employed to estimate V_{av} from the ratio V_{av}/Vs_{av}, the velocity coefficient, where Vs_{av} is the average surface velocity obtained by the image velocimetry algorithm. The established practice [34] for estimating the average cross-sectional flow velocity from the surface velocity is to assume a velocity coefficient equal to 85%.

Table 2: Average flow velocity V_{av}, average surface flow velocity Vs_{av}, estimate of V_{av} based on 0.85 Vs_{av}, 20th percentile of the empirical distribution V_{EMP} and the theoretical V_{DIS}, and relative errors of the these three estimators.

Case study	V_{av} (m/s)	Vs_{av} (m/s)	0.85 Vs_{av} (m/s)	V_{EMP} (m/s)	V_{DIS} (m/s)	Error 0.85 Vs_{av} (%)	Error V_{EMP} (%)	Error V_{DIS} (%)
Loussios	0.89	1.04	0.88	0.82	0.83	-1	-8	-7
Nedousa	0.93	1.32	1.12	1.06	1.04	20	14	11
Nedontas	2.75	3.35	2.85	2.65	2.58	4	-4	-6

The errors of these three estimators are displayed in Table 2. The last three columns (the error is calculated from the formula $V_{est}/V_{av} - 1$, where V_{est} is either 0.85 Vs_{av}, or V_{EMP}, or V_{DIS}) suggest that, judging from all three case studies, our method is slightly advantageous (lower uncertainty regarding the error, although this is based on just 3 case studies). The use of the theoretical distribution instead of the empirical distribution offers a minor improvement. However, since the former requires specialized commercial software, the use of the empirical remains a good alternative.

5. Conclusions

This study presented an image velocimetry algorithm. The algorithm was tested in four case studies with different camera angles. The algorithm has been implemented in MATLAB code (also compatible with the open-source platform Octave). The results of the case studies indicate that this algorithm provided a good estimation of the surface flow velocity (both the magnitude and direction), and the profile along the cross-section. Furthermore, though not extensively examined, the algorithm appears to be faster than other interpreter-based tools.

The presented tool, which is freely available, provided reliable estimations of the surface flow velocities in the case studies of this work. An alternative approach for estimating the average flow velocity of the cross-section was examined. This approach employs the surface velocity of 20% non-exceedance probability. This methodology appeared promising when LSPIV was applied to videos with high seeding density. These findings should be tested more extensively in a series of case studies with a variety of conditions to identify their potential in field applications.

Author Contributions: Conceptualization, E.R. and P.D.; methodology, E.R.; software, E.R.; validation, A.K. and K.M.; formal analysis, E.R.; resources, K.M.; data curation, S.L.; writing—original draft preparation, E.R.; writing—review and editing, A.K. and P.D.; visualization, E.R.; supervision, E.R. and A.K.; project administration, K.M.; funding acquisition, K.M. All authors have read and agreed to the published version of the manuscript.

Funding: The authors acknowledge the funding from the Hellenic General Secretariat for Research & Technology, under the National Strategic Reference Framework (2014-2020), for the project HYDRO-NET: Hydro-Telemetric Networks of Surface Waters: Gauging instruments, smart technologies, installation and operation, as a part of the Hellenic Integrated Marine and Inland Water Observing, Forecasting and Offshore Technology System, HIMIOFoTS (MIS5002739).

Conflicts of Interest: The authors declare no conflict of interest.

References

1. Wang, Y.; Hsu, Y.; You, G.; Yen, C.; Wang, C. Flood Inundation Assessment Considering Hydrologic Conditions and Functionalities of Hydraulic Facilities. *Water* **2018**, 10, 1879.
2. Rozos, E. A methodology for simple and fast streamflow modelling. *Hydrological Sciences Journal* **2020**, 65, 1084-1095.
3. Rozos, E. Machine Learning, Urban Water Resources Management and Operating Policy. *Resources* **2019**, 8, 173.
4. World Meteorological Organization. *Manual on stream gaugin vol. I Fieldwork*, WMO-No.1044, Geneva, Switzerland, 2010.
5. Hauet, A. Stream Gauging Techniques, In Course on Stream Gauging, IAHR WMO IAHS Training, Lyon, September 2-4, 2018.
6. Kasvi, E.; Laamanen, L.; Lotsari, E.; Alho, P. Flow Patterns and Morphological Changes in a Sandy Meander Bend during a Flood—Spatially and Temporally Intensive ADCP Measurement Approach. *Water* **2017**, 9, 106.
7. Chiu, C.L. Entropy and 2-D velocity in open channels. *J. Hydraul. Eng*. **1988**, 114, 738–756.
8. Dimitriadis, P.; Koussis, A.; Koutsoyiannis, D. Estimating the hydraulic profiles in a cross-section under one-dimensional steady-flow dynamics by employing the entropy maximization principle: I. Theoretical concepts, *RG* **2019**, DOI: 10.13140/RG.2.2.10168.29441/1.
9. Dimitriadis, P.; Rozos, E.; Mazi, K.; Koussis, A. Estimating the hydraulic profiles in a cross-section under one-dimensional steady-flow dynamics by employing the entropy maximization principle: II. Applications, *RG* **2019**, 10.13140/RG.2.2.16879.18088/2.
10. Manfreda, S.; McCabe, M. Emerging Earth Observing Platforms Offer New Insights Into Hydrological Processes, *Hydrolink* **2019**, 1, 8-9.
11. Pearce, S.; et al. An Evaluation of Image Velocimetry Techniques under Low Flow Conditions and High Seeding Densities Using Unmanned Aerial Systems, *Remote Sens.* **2020**, 12(2), 232; doi:10.3390/rs12020232.
12. Fujita, I. Discharge Measurements of Snowmelt Flood by Space-Time Image Velocimetry during the Night Using Far-Infrared Camera. *Water* **2017**, 9, 269.
13. Koutalakis, P.; Tzoraki, O.; and Zaimes, G. UAVs for Hydrologic Scopes: Application of a Low-Cost UAV to Estimate Surface Water Velocity by Using Three Different Image-Based Methods, *Drones* **2019**, 3, 14; doi:10.3390/drones3010014.
14. Thielicke, W. PIVlab – particle image velocimetry (PIV) tool, MATLAB Central File Exchange. Available online: https://tinyurl.com/wmnzokj (accessed on 5 February 2020).
15. Le Coz, J.; Jodeau, M.; Hauet, A.; Marchand, B.; and Le Boursicaud, R. Image-based velocity and discharge measurements in field and laboratory river engineering studies using the free Fudaa-LSPIV software. *Proceedings of the International Conference on Fluvial Hydraulics, RIVER FLOW* **2014**, 1961–1967.
16. Fujita, I.; Muste, M.; Kruger, A. Large-scale particle image velocimetry for flow analysis in hydraulic engineering applications, *Journal of Hydraulic Research* **1998**, Vol.36, No.3, pp.397-414.
17. Muste, M.; Fujita, I.; and Hauet, A.Large-scale particle image velocimetry for measurements in riverine environments. *Water Resources Research* **2008**. 44, 1 – 14, doi:10.1029/2008WR006950. W00D19.
18. Le Boursicaud, R.; Pénard, L.; Hauet, A.; Thollet, T.; and Le Coz, J.; Gauging extreme floods on YouTube: application of LSPIV to home movies for the post-event determination of stream discharges. *Hydrol. Process.* **2016**, 30, 90–105.
19. Dramais, G.; Le Coz, J.; Camenen, B.; and Hauet, A. Advantages of a mobile LSPIV method for measuring flood discharges and improving stage-discharge curves. *Journal of Hydro-Environment Research* **2011**, 50(4): 301– 312.
20. Le Coz, J.; Hauet, A.; Pierrefeu, G.; Dramais, G.; Camenen, B. Performance of image-based velocimetry (LSPIV) applied to flash-flood discharge measurements in Mediterranean rivers. *Journal of Hydrology* **2010**., 394, 42 – 52, doi:10.1016/j.jhydrol.2010.05.049.
21. Kantoush, S.A.; Schleiss, A.J.; Sumi, T.; and Murasaki, M. LSPIV implementation for environmental flow in various laboratory and field cases, *J. Hydro-Environment Res*. **2011**, 5(4), 263–276.
22. Rozos, E. Simple image velocimetry, HydroShare, Available online (accessed on 25 February 2020) https://tinyurl.com/t8dxa8q
23. Chen, Y.C.; Hsu, Y.C.; Kuo, K.T. Uncertainties in the Methods of Flood Discharge Measurement, *Water Resour. Manag*. **2013**, 27, pp. 153–167.

24. Fulton, J.; Ostrowski, J. Measuring real-time streamflow using emerging technologies: Radar, hydroacoustics, and the probability concept, J. *Hydrol.* **2008**, 357(1), 1–10.
25. Thielicke, W.; Stamhuis, E.J. PIVlab – Towards User-friendly, Affordable and Accurate Digital Particle Image Velocimetry in MATLAB. *Journal of Open Research Software* **2014**, 2: e30, DOI: 10.5334/jors.bl.
26. Shapiro, L.G.; Stockman, G.C. *Computer Vision*, The University of Washington, Seattle, Washington, 2000; pp. 166-170.
27. Lewis, J.P. Fast Template Matching, *Vision Interface* **1995**, pp. 120-123.
28. Goshtasby, A. Image registration by local approximation methods, *Image and Vision Computing* **1988**, 6, pp. 255-261.
29. Karsli, F.; Dihkan, M. Determination of geometric deformations in image registration using geometric and radiometric measurements, *Academic Journal* **2010**, 5(3), pp. 260-274.
30. Novak, K. Rectification of digital imagery, *Photogrammetric Eng. Remote Sensing* **1992**, 58(3), pp. 339-344.
31. Koutsoyiannis, D. *Probability and statistics for geophysical processes*, doi:10.13140/RG.2.1.2300.1849/1, National Technical University of Athens, Athens, **2008**.
32. Anderson, T.W.; Darling, D.A. Test of Goodness-of-Fit. *Journal of the American Statistical Association* 1954. 49: 765–769.
33. Boos, D.D. Minimum anderson-darling estimation, *Communications in Statistics - Theory and Methods* **1982**, 11:24, 2747-2774, DOI: 10.1080/03610928208828420.
34. Rantz, SE. 1982. *Measurement and computation of streamflow. In Measurement of Stage and Discharge, Vol. 1*, Water-Supply Paper 2175. US Geological Survey: Washington, pp. 137.